JOURNAL OF GEOPHYSICAL RESEARCH, VOL. 102, NO. D5, PAGES 6117–6129, MARCH 20, 1997

Dynamical proxies of column ozone with applications to global trend models

J. R. Ziemke [1]

National Research Council, NASA Goddard Space Flight Center, Greenbelt, Maryland

S. Chandra, R. D. McPeters, and P. A. Newman

NASA Goddard Space Flight Center, Greenbelt, Maryland

Abstract. Previous regression trend models for total column ozone have included only the quasi-biennial oscillation (QBO) winds and the El Niño Southern Oscillation (ENSO) ocean surface pressure as dynamical proxies. Trends derived from these regression models generally differ (are more negative) from two-dimensional (2-D) chemical transport trends by about 2-5% decade^{-1} in midlatitudes during spring. The present study introduces additional dynamical proxies of total ozone in regression models in an effort to reduce errors in local ozone trends and reduce these model differences. Nimbus 7 total ozone mapping spectrometer (TOMS) version 7 total column ozone for 1979–1992 are used in conjunction with analyses from National Centers for Environmental Prediction (NCEP, formerly National Meteorological Center). Dynamical proxies investigated include winds (including diabatic winds), relative vorticity, potential vorticity, temperatures, and geopotential heights. Inclusion of additional dynamical proxies improves statistics by reducing residuals and uncertainty regions in both zonal mean and zonally asymmetric trend models. RMS reductions, relative to a trend model with only QBO, solar, and trend terms, are as large as 50% in 14-year means in the southern hemisphere. For zonal mean or zonally asymmetric global trend models with one optional surrogate, a favorable choice is prefiltered (at least deseasonalized and detrended) lower stratospheric temperatures. Relative vorticity, potential vorticity, and geopotential heights all exhibit similar relationships with total ozone, with highest correlative behavior near 200 hPa (midlatitudes year-round) and 10 hPa (high latitudes in winter-spring months). For models incorporating these latter proxies, combined 10- and 200-hPa (or similar) pressure levels are effective in reducing global residuals. ENSO, as a surrogate by itself or included with other dynamical proxies, has a comparatively small effect because of its episodic nature. Decadal variabilities in NCEP and microwave sounding unit channel 4 (MSU4) data as surrogates in trend models indicate maximal 1-3% decade^{-1} reductions anywhere in TOMS trends. Total ozone trends derived from the Goddard 2-D heterogeneous chemistry and transport model agree favorably with trends in TOMS ozone, generally to within 2-3% decade^{-1} in both hemispheres. Inclusion of possible decadal variabilities in dynamics may yield yet smaller differences.

1. Introduction

Many studies in recent years have applied specially designed regression models in an effort to determine global characteristics of anthropogenic trends in ozone [e.g., *Stolarski et al.*, 1991, 1992; *Niu et al.*, 1992; *Randel and Cobb*, 1994; *Reinsel et al.*, 1994].

In addition there have been many two-dimensional (2-D) heterogeneous chemical transport models used to delineate long-term trends in ozone [see, for example, World Meteorological Organization (*WMO*), 1995; *Solomon et al.*, 1996; *Jackman et al.*, 1996]. Comparison of trends derived from 2-D chemical transport models and total ozone mapping spectrometer (TOMS) regression models have characteristically shown disagreements in the northern hemisphere (NH), with TOMS indicating more negative values, not uncommonly 2-5% decade^{-1} more negative. Version 6 TOMS trend analyses by *Stolarski et al.* [1991] showed trends between −8% and −10% decade^{-1} in NH midlatitudes

[1]Also at Software Corporation of America, Lanham, Maryland.

Paper number 96JD03783.
0148-0227/97/96JD-03783$09.00

around February. In contrast, 2-D transport models typically show NH midlatitude trends around −2% to −4% decade^{-1}. TOMS trends also exhibit a midlatitude maximum in NH spring that 2-D transport models do not reproduce. In this study we compare trends derived from 2-D transport models and TOMS ozone.

Two components not present in 2-D heterogeneous transport models are interannual and possible decadal changes in ozone caused by atmospheric dynamics. Evidence of dynamically induced longitudinal distributions of NH TOMS trends in winter-spring was shown by *Hood and Zaff* [1995] for January months using National Centers for Environmental Prediction (NCEP) data (primarily 100-hPa geopotential heights) and by *Chandra et al.* [1996] in northern midlatitudes using microwave sounding unit channel 4 (MSU4) and NCEP data. The main implication was that longitudinal structures of NH total ozone trends during winter-spring were a result of stationary planetary scale waves in the troposphere and lower stratosphere. Most regression trend models include at least an 11-year solar cycle and the quasi-biennial oscillation (QBO) as natural sources of ozone variability. Recent models have also included seasonal time dependence in regression coefficients, and other nonanthropogenic variability sources including the El Niño-Southern Oscillation (ENSO) [*Randel and Cobb*, 1994] and atmospheric temperatures [*Chandra et al.*, 1996]. In addition, aerosols from the eruptions of El Chichon in April 1982 and Mount Pinatubo in June 1991 were shown by *Solomon et al.* [1996] to have an important effect on both decadal trends as well as interannual variabilities in total ozone in NH midlatitudes. In this study we employ dynamical parameters in regression models to reduce residual errors and to estimate the long-term impact of decadal dynamical variabilities on global structures and amplitudes of ozone trends. Additional dynamical parameters include winds (including diabatic winds), relative vorticity, potential vorticity, temperatures, and geopotential heights. We do not attempt to model variabilities in total ozone caused by naturally occurring aerosols. Missing effects from aerosols will manifest themselves in derived residuals and as errors in trends.

This paper is composed of five remaining sections. Sections 2–4 discuss data, a generalized trend model, and dynamical proxies of total ozone, respectively. Section 5 includes applications of zonal mean and zonally asymmetric regression trend models. Last, section 6 provides a summary.

2. Data

Total column ozone used in this study are Nimbus 7 version 7 TOMS data for January 1, 1979, through December 31, 1992. Standard atmospheric variables, including temperatures, relative vorticity, and winds (including diabatic winds) and other computed quantities for this same time period, were all derived from daily (1200 UTC) standard National Centers for Environmental Prediction geopotential height analyses on pressure surfaces 1-850 hPa. Relative vorticity is defined as the vertical component of the three-dimensional (3-D) curl of wind velocity. That is, relative vorticity is defined as $v_x - u_y$, where v and u represent northward and eastward wind components, respectively, and subscripts denote partial differentiation (eastward and northward distances are x and y, respectively). Daily diabatic winds in this study were derived from NCEP temperatures and diabatic heating rates (J. Rosenfield, personal communication, 1996) using the iterative method of *Murgatroyd and Singleton* [1961]. In addition, microwave sounding unit channel 4 brightness temperatures (half-vertical weighting function response near 40 and 150 hPa, mean near 90 hPa) were also incorporated in this study.

For both consistency and error reduction, all daily data were binned to equivalent 5° latitude (85°S to 85°N) by 15° longitude block structures. Missing and/or outlier data were replaced using a 3-D (latitude, longitude, day) Gaussian weighting procedure (similar to that used by *Stone et al.* [1995]), followed by linear interpolation in time. All data were subsequently averaged monthly to reduce computational effort in our regression trend models.

Monthly mean zonal winds from Singapore (1°N, 140°E) from 1979 through 1992 at pressure levels 70, 50, 40, 30, 20, 15, and 10 hPa were used to provide a QBO index in our regression trend models (discussed in section 3.1). A Tahiti (18°S, 150°W) minus Darwin (13°S, 131°E) monthly mean normalized sea level pressure time series for the same time period was used as an ENSO proxy, and for a solar ultraviolet (UV) index, monthly mean 10.7-cm solar flux time series was incorporated. Prior to trend analyses, all 1979-1992 time series averages were removed from the QBO, ENSO, and solar flux series.

3. Generalized Regression Model

Methods used in recent years to determine trends in global total ozone have used regression models similar to that of *Stolarski et al.* [1991]. Several studies [e.g., *Stolarski et al.*, 1992; *Niu et al.*, 1992; *Randel and Cobb*, 1994] have extended the method to include zonally asymmetric data. The models prescribed simple linear relationships between total ozone and surrogates, an assumption that is viable as a first approximation. Subtle nonlinear effects were not included.

All of these regression models usually included a linear trend term, QBO, solar flux series, and for *Randel and Cobb* [1994], an additional ENSO proxy. In this study of both zonal mean and zonally asymmetric data, we incorporate a similar model including ENSO (an option, for zonally asymmetric data), and in addition, optional surrogates $\mathrm{P}_1(t)$ and $\mathrm{P}_2(t)$:

$$\Omega(t) = \alpha + \beta\, t + \gamma\ \mathrm{QBO}(t) + \delta\ \mathrm{solar}(t) + \epsilon\ \mathrm{ENSO}(t) + \zeta_1\ \mathrm{P}_1(t) + \zeta_2\ \mathrm{P}_2(t) + \mathrm{R}(t). \quad (1)$$

In (1), t is the month index (t=1,2,...,168), and $\alpha, \beta, \gamma, \delta, \epsilon, \zeta_1$, and ζ_2 are time-dependent regression coefficients given by a constant plus 12-month, 6-month, and 4-month cosine and sine harmonic series as defined by *Randel and Cobb* [1994]. That is, α (similar expression for the other coefficients) is given by the harmonic expansion $c_0 + \sum_{j=1}^{3}[c_j \cos(2\pi jt/12) + s_j \sin(2\pi jt/12)]$, where c_j and s_j are constant coefficients. The purpose of providing annual (plus two harmonics) variability in these regression coefficients is to allow more physically realizable seasonality. The error in model (1) is the residual series R(t), α is the seasonal fit, and the ozone trend is given by the coefficient β. Solar(t) in (1) represents the solar proxy (10.7-cm solar flux series), and ENSO(t) is given by the Tahiti minus Darwin normalized sea level pressure time series. QBO(t) in (1) represents the quasi-biennial oscillation proxy derived from Singapore (1°N, 140°E) zonal winds using several approaches, including that of *Randel et al.* [1995] (discussed in section 3.1). Error analysis for the regression coefficients involved a Monte Carlo method and is discussed in the appendix.

3.1. Choosing a Representation for QBO

Excluding effects from volcanic aerosols, interannual variabilities in total ozone in the tropics and subtropics are primarily driven by a slow secondary stratospheric circulation associated with the QBO. Several studies [e.g., *Hasebe*, 1980, 1994; *Bowman*, 1989; *Lait et al.*, 1989; *Hamilton*, 1989; *Chandra and Stolarski*, 1991] have shown that QBO anomalies in total ozone maximize along the equator with amplitudes ~6-10 DU (Dobson units) and in the subtropics in winter-spring months with amplitudes ~6-12 DU. Vertical motion associated with the QBO during the eastward transition phase (largest positive vertical derivative of the QBO zonal winds) is, by near-geostrophic thermal wind balance, characterized by sinking motion along the equator and upwelling in the subtropics [*Andrews et al.*, 1987]. Sinking motion brings larger ozone mixing ratio downward from the middle stratosphere, producing enhanced total column ozone anomalies. For rising motion, the opposite happens. During the westward transition phase of the QBO, these wind fields and their effect on total ozone reverse.

There are many possible representations of QBO(t) in (1), from simply using a single level of Singapore winds to more involved approaches, perhaps including multiple least squares or empirical orthogonal function (EOF) analysis. We compare two methods that seem to yield the general spread of residual reductions possible with the choice of QBO(t) within model (1). The first is a simplistic approach using 30-hPa Singapore winds without time lag and the other is an EOF method.

The representation for QBO(t) used by *Randel et al.* [1995] was the EOF approach introduced by *Wallace et al.* [1993]. (A thorough description of the general EOF method is provided by *Kutzbach* [1967].) Following *Wallace et al.* [1993], QBO(t) is given by

$$\mathrm{QBO}(t) = [c_1(t)^2 + c_2(t)^2]^{1/2} \cos[\Phi(t) - \lambda], \quad (2)$$

where $c_1(t)$ and $c_2(t)$ are time series associated with the two leading eigenvalues, $\Phi(t)$ is a four-quadrant phase series defined by $\tan[\Phi(t)] = c_2(t)/c_1(t)$, and λ is a constant phase lag to be determined. For 1979-1992 Singapore winds, the two leading eigenfunctions explain 95% of total variance of the vertical QBO structure. One of our methods, similar to that of *Randel et al.* [1995], was to adjust the phase lag λ in (2) to maximize cross correlation with the QBO signal in equatorial TOMS ozone, using the same value for λ at all other latitudes. As will be shown, this EOF representation for QBO(t) does as well anywhere compared with computing a new λ at each latitude (hereinafter denoted as lagged EOF QBO winds), and much better than using 30-hPa nonlagged Singapore winds.

In Figure 1 we compare 14-year averaged RMS residual patterns for these two representations, beginning with a standard global trend model (see dotted curve) from (1) that uses zonal mean data and is defined by only seasonality, linear trend, and solar cycle terms (that is, $\Omega(t) = \alpha + \beta\, t + \delta\ \mathrm{solar}(t) + \mathrm{R}(t)$.). In the tropics, 14-year residual RMS amplitudes for this simplest model are seen to maximize along the equator (~7 DU amplitude), with relative minima at 10°N and 10°S. Outside the tropics, residual amplitudes in the southern hemisphere (SH) polar region are largest, growing to ~10 DU at 65°S.

Extending the standard model to now include nonlagged 30-hPa Singapore winds (light solid curve in Figure 1) provides RMS residual reductions of around 2-3 DU in the tropics and SH subtropics. For the EOF QBO winds, there is little difference between using the

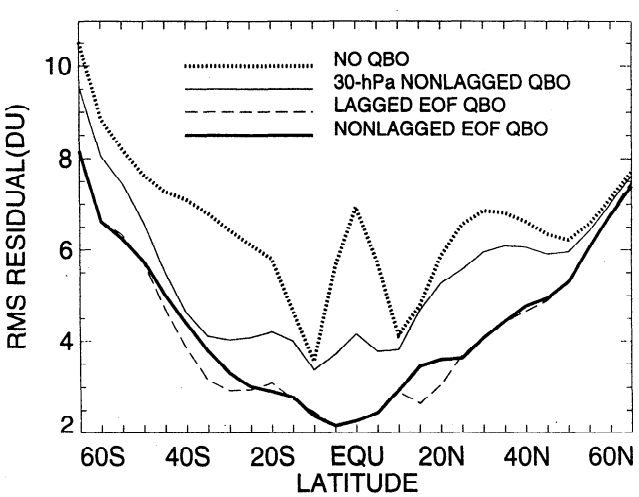

Figure 1. RMS residuals (in Dobson units) in zonal mean trend model with no quasi-biennial oscillation (QBO) (bold dashed curve), 30-hPa nonlagged Singapore QBO winds (light solid curve), lagged empirical orthogonal function (EOF) QBO winds (long dashed curve), and nonlagged EOF QBO winds (bold solid curve). The trend model used is $\Omega(t) = \alpha + \beta\, t + \gamma\ \mathrm{QBO}(t) + \delta\ \mathrm{solar}(t) + \mathrm{R}(t)$.

lagged (long dashed curve) or nonlagged (bold solid curve) method. The EOF QBO winds show marked improvements from using the nonlagged 30-hPa Singapore winds, with larger residual reductions (~2-5 DU) from the standard (no QBO) model. Figure 1 shows 5-DU improvement (~60-70%) along the equator using the EOF QBO winds. In all trend models used in this study we incorporated the nonlagged EOF QBO representation.

3.2. ENSO and Residuals

Another interannual dependence in total ozone, one that extends from the tropics to high latitudes, comes from ENSO. As *Randel and Cobb* [1994] showed, ENSO anomalies in zonally asymmetric total ozone are largest in the middle and high latitudes and occur during winter-spring months, the reason being that in wintertime the tropospheric eastward wind jet lies closer toward the equator, enabling larger radiation of tropical waves (primarily westward propagating Rossby-type responses in the troposphere) into the winter extratropics [*Garcia and Salby*, 1987]. *Randel and Cobb* [1994] found that ENSO-associated changes in total ozone in middle and high latitudes appear as sharply defined events that coincide (inphase) with similar sharp episodic changes in lower stratospheric temperatures. Anomalies [*Randel and Cobb*, 1994, Figure 14] in SH midlatitudes were shown to exceed 15 DU in total ozone and 2 K in MSU4 temperatures, yielding a sensitivity ratio of around 6-9 DU K^{-1}, which is indicative of dynamical forcing. We note in addition that their ozone-temperature residuals (their Figure 15) indicated similar sensitivity ratios.

The impact of including ENSO in zonally asymmetric models for reducing residuals is shown in Figure 2. The trend model used is $\Omega(t) = \alpha + \beta\, t + \gamma\ \mathrm{QBO}(t) + \delta\ \mathrm{solar}(t) + \epsilon\ \mathrm{ENSO}(t) + \mathrm{R}(t)$. Figure 2 (top) shows global RMS residuals in TOMS ozone, annually averaged, assuming no ENSO. Largest residual errors occur in the high latitudes of both hemispheres, exceeding 12 DU. When ENSO is included (Figure 2, bottom) the net effect is surprisingly small in reducing residuals, with reductions around only 1 DU or less. The reason for the small reductions stems from the episodic nature of ENSO, where appreciable amplitudes appear only in 1982-1983, 1987–1989, and 1991–1992 [*Randel and Cobb* [1994].

As shown later in section 5, much larger residual reductions are possible with the inclusion of other (optional) dynamical surrogates of ozone. In the next section we will examine several of these and their dynamical relationships with total ozone.

4. Optional Dynamical Proxies: Correlation Cross Sections

Understanding Ω-T relationships is vital for assessing relative contributions to total ozone change from dynamics and radiative feedback effects. This is because dynamical surrogates of total ozone are derived ultimately from retrieved atmospheric temperatures. Investigations such as *Shine* [1986], *Kiehl et al.* [1988], and *Miller et al.* [1992] indicated around 15-20 DU K^{-1} relative change ratio (sensitivity) between total ozone and lower stratospheric temperatures when ozone loss is imported as the cause of temperature loss (i.e., radiative feedback). In contrast, other studies such as *Newman and Randel* [1988] and *Randel and Cobb* [1994, and references therein] showed around 6-10 DU K^{-1} sensitivity of total ozone to lower stratospheric temperature based on dynamical forcing. In our study, sensitivity ratios (figures not shown) between filtered (deseasonalized and linearly detrended) monthly mean TOMS total ozone and NCEP temperatures indicate largest values anywhere of 5-7 DU K^{-1} in the lower stratosphere in both hemispheres. In addition, on timescales varying up to several months, *Chandra et al.* [1996] showed that there is little temporal phase shift observed between total ozone and lower stratospheric temperatures, further suggesting a greater impact from dynamical forcing. A thorough study comparing dynamical and radiative effects on global Ω has yet to be shown. In accordance with results from previous investigations, the filtered monthly mean surrogate fields used in this study indicate predominant dynamical, rather than radiative, control on ozone variability. This may not be the case where surrogates are not detrended (discussed in section 5.3).

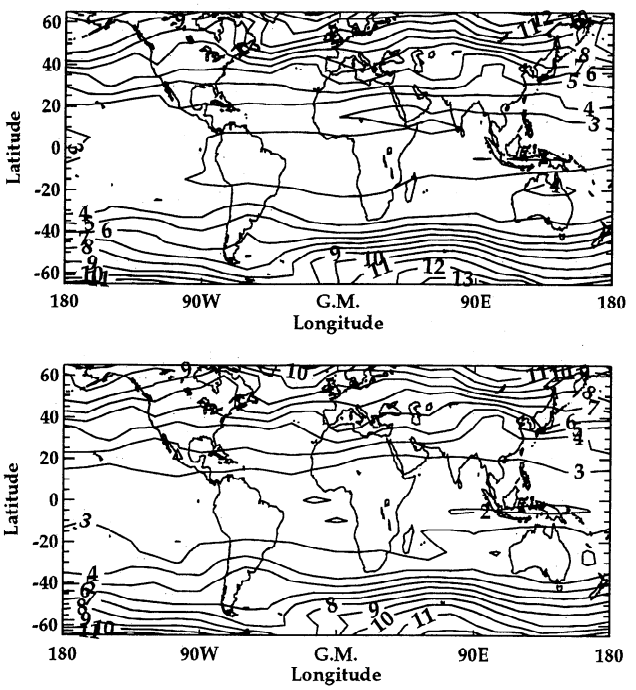

Figure 2. RMS residuals (in Dobson units averaged for 1979-1992) for a zonally asymmetric trend model with no El Niño Southern Oscillation (ENSO) (top) and with ENSO (bottom). The trend model used is $\Omega(t) = \alpha + \beta\, t + \gamma\ \mathrm{QBO}(t) + \delta\ \mathrm{solar}(t) + \epsilon\ \mathrm{ENSO}(t) + \mathrm{R}(t)$.

In an effort to identify dynamical surrogates of total ozone, standard correlation between monthly 2-D

TOMS ozone and 3-D atmospheric variables was calculated at each grid point (i.e., each latitude, longitude, pressure) after removing time series averages, from

$$[\sum_{t=1}^{N}\Omega(t)\mathrm{P}(t)]/[\sum_{t=1}^{N}\Omega(t)^2\sum_{t=1}^{N}\mathrm{P}(t)^2]^{1/2}, \quad (3)$$

where N is 168 months, and Ω and P denote TOMS total ozone and 3-D variable time series, respectively. Prior to calculations, all time series were deseasonalized and linearly detrended. Detrending ensures that decadal timescale radiative feedback effects will not be present. Deseasonalization was accomplished by first deriving a 14-year seasonal (12-month periodicity) time series by averaging similar months together, followed by subtracting this from the original data series.

Figure 3 shows 1979-1992 vertical cross sections of zonally averaged correlations between TOMS total ozone and several basic dynamical surrogates. We note that there is a clear seasonality of strongest correlations, especially in the high-latitude stratosphere in winter-

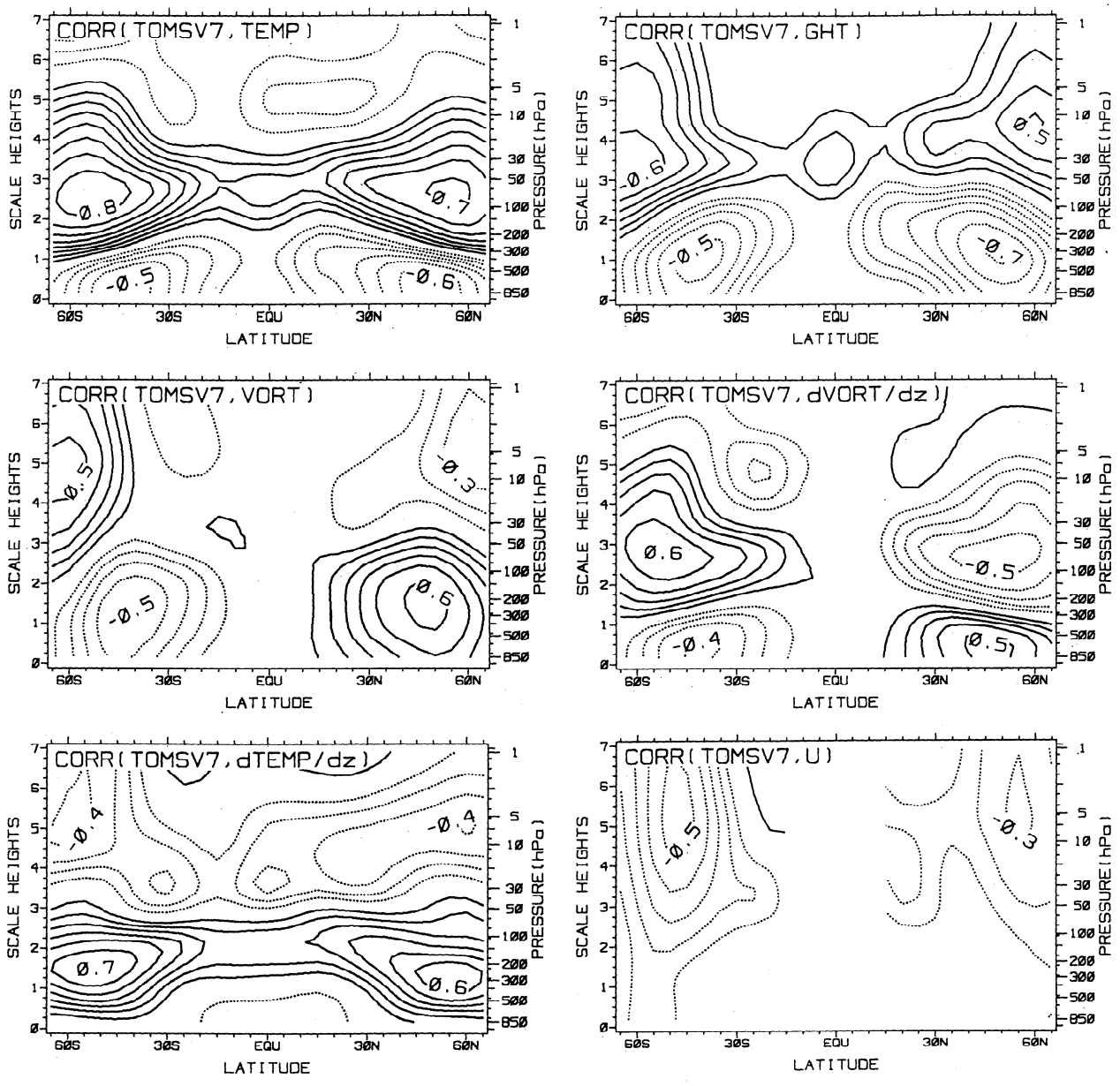

Figure 3. Zonally averaged vertical cross correlations between several three-dimensional (3-D) (latitude, longitude, pressure) atmospheric quantities and two-dimensional (2-D) (latitude, longitude) total ozone mapping spectrometer (TOMS) total ozone. Dashed (solid) contour values start at -0.1 (0.1) and decrement (increment) by 0.1. One scale height represents 7 km. Correlations were calculated (see text) at each grid point using deseasonalized, detrended monthly mean data for 1979–1992 (168 months). Monte Carlo simulations of 100,000 data runs, modeling both TOMS ozone and surrogate series as Markov noise with an upper bound redness parameter 0.999 [*Stanford and Ziemke*, 1994], indicate that correlations are statistically significant at the 1% significance level for absolute values greater than 0.4.

spring months in both hemispheres (figures not shown). For conciseness, correlation fields in Figure 3 include all months averaged together.

Correlation patterns between TOMS ozone and NCEP temperatures (top panel, left column) in Figure 3 maximize in middle and high latitudes, with large positive correlations in the lower stratosphere and negative correlations in the low to middle troposphere. Zero correlations are seen tracking along the tropopause from about 100 to 200 hPa in low latitudes downward to ~300 hPa in high latitudes. Observations of strong correlations between atmospheric temperature and total ozone are not new [*Dobson and Harrison*, 1926; *Dobson et al.*, 1946; *Reed*, 1950]. Background distributions of ozone mixing ratio and temperature are such that the combination of both horizontal and vertical parcel motions create the observed correlation fields between total ozone and atmospheric temperature [see, for example, *Newman and Randel*, 1988; *Wirth*, 1993].

Correlations between geopotential heights and TOMS ozone (top panel, right column) also maximize in middle and high latitudes. Large negative correlations appear in midlatitudes in both hemispheres near the tropopause. These negative correlations occur yearround because of the persistent tropospheric wind jet, where relative maxima in stratospheric column integrated ozone will be found within upper tropospheric cyclonic (low pressure) regions. For geopotential heights, lower than average geopotential heights near the tropopause cause a higher than average mass density and a larger vertically integrated column ozone anomaly, thereby yielding the negative correlations seen in Figure 3. Positive correlations occur in the stratosphere in high latitudes of both hemispheres and are caused by vertically propagating planetary waves, primarily in the winter and spring months. (*Wirth* [1993] has analyzed such planetary waves and their effects on ozone for the SH vortex in October.) Opposite signs in correlations observed in both hemispheres between the tropopause (~200-300 hPa) and the midstratosphere (~30 hPa) can be understood on the basis of the 3-D structures of vertically propagating temperature waves. Since geopotential heights are equivalent to vertically integrating temperatures in log-pressure height, these sign differences can be interpreted as a combination of both vertical tilt (generally westward tilt with height) of the waves and fundamentally opposing zonal mean meridional temperature gradients at these altitudes in winter-spring.

The correlation field involving relative vorticity (middle panel, left column) is similar to the field between TOMS ozone and geopotential heights except for a distinct sign change between hemispheres. We note that Ertel potential vorticity (EPV) yields correlation patterns (not shown) that are virtually the same as those using relative vorticity in Figure 3, the reason being the physical nature of vorticity. In upper tropospheric cyclonic regions, high total ozone coincides with high (low) values of relative vorticity and EPV in the NH (SH). Opposite signs in the correlation patterns between NH and SH occur because winds flow counterclockwise around low-pressure cells in the NH and clockwise around lows in the SH. Hence, for either EPV or relative vorticity in midlatitudes near the tropopause, positive anomalies in the NH and negative anomalies in the SH will correlate with positive anomalies in column ozone.

Patterns involving the vertical derivative of relative vorticity (middle panel, right column) are similar to the patterns involving temperatures, except for the sign change between hemispheres discussed previously. Besides being representative of atmospheric temperature anomalies, the vertical derivative of relative vorticity also provides a crude indicator of vertical motion, with upwelling coinciding with negative (positive) vertical gradients of relative vorticity in the NH (SH).

Another dynamical surrogate of column ozone is the vertical derivative of temperature using log-pressure as the vertical coordinate (bottom panel, left column). Maximum (positive) correlations are seen to track along the tropopause, from around 100 to 200 hPa in the tropics downward to around 300 hPa in high latitudes. A positive value of the vertical derivative of temperature at fixed pressure near the tropopause (for example, at 200 hPa in midlatitudes) indicates descending stratospheric air; a positive correlation with total ozone follows because the descending air creates a positive anomaly in stratospheric column ozone.

As a final example, we consider stratospheric winds. A strong wind structure can produce a barrier against transport into and out of the vortex. Dynamical structures during winter-spring middle to high latitudes in both hemispheres usually show large variability with altitude (generally strong westward tilt with height). In addition, strong wind anomalies will occur away from the pole of the vortex, at some altitude coinciding with strong zonal anomalies (of opposite sign) in TOMS ozone. The result is negative correlations between zonal winds in the upper stratosphere at high latitudes in Figure 3 (bottom panel, right column).

The results from Figure 3 depict only a small portion of possible dynamical surrogates of total ozone. In this study we include several of these surrogates (and several others not shown) in our regression trend models.

5. Applications of Optional Dynamical Proxies in Trend Models

5.1. Residuals: Zonal Mean Models

Despite zonally asymmetric data used to generate correlation cross sections in Figure 3, similar patterns and amplitudes still persist for zonal mean data (figure not shown). Selected zonal mean time series plotted in Figure 4 correspond to regions of largest correlation amplitudes in Figure 3. Surrogate time series (light solid curves) were deseasonalized, linearly detrended, and then zonally averaged. In an effort to more clearly identify correlative relationships between surrogates and TOMS ozone for use in zonal mean trend models, the seasonal cycle, QBO, solar cycle, and long-term trend were removed from each TOMS series, resulting in the TOMS residuals (bold

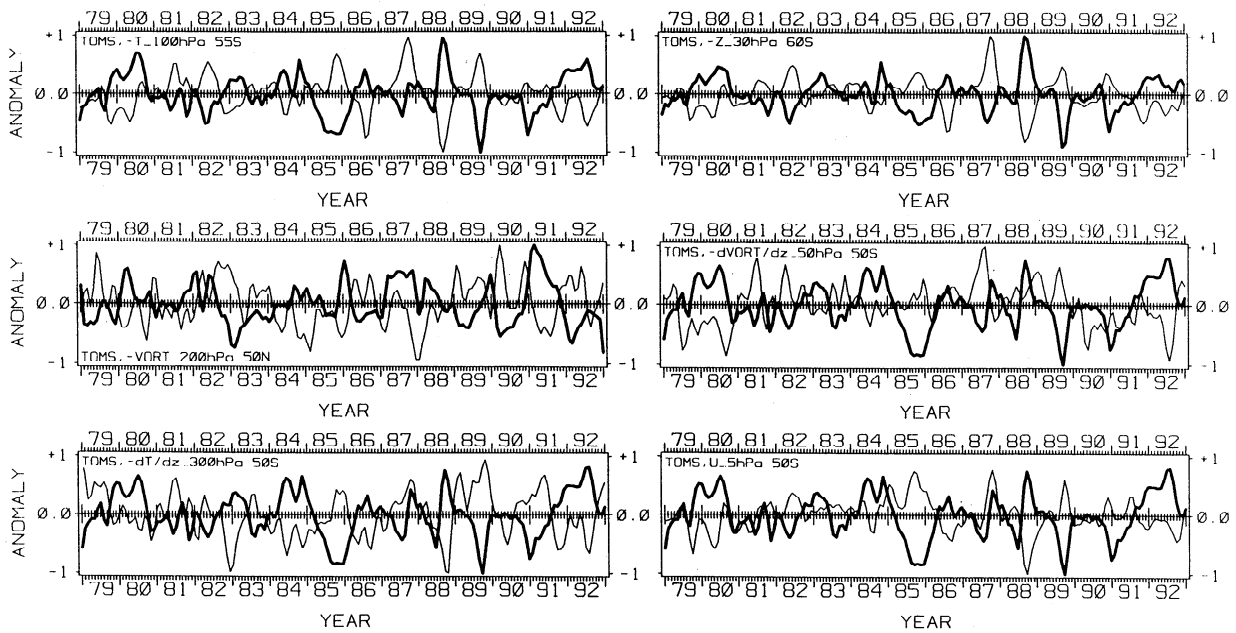

Figure 4. Normalized (maximum amplitude = 1) monthly time series of total ozone residuals R(t) (bold curves) plotted against normalized surrogates (light curves) for regions (latitudes and pressures indicated) of large correlation amplitudes seen in Figure 3. No units. Prior to trend analyses, surrogate time series (light solid curves) were deseasonalized, linearly detrended, and then zonally averaged. Several surrogate series were multiplied by -1 (indicated) for clarity. R(t) was derived from the zonal mean trend model $\Omega(t) = \alpha + \beta\, t + \gamma\ \mathrm{QBO}(t) + \delta\ \mathrm{solar}(t) + \mathrm{R}(t)$ (see section 5.1.).

curves) shown in Figure 4. The TOMS residual series R(t) was derived from the zonal mean trend model $\Omega(t) = \alpha + \beta\, t + \gamma\ \mathrm{QBO}(t) + \delta\ \mathrm{solar}(t) + \mathrm{R}(t)$. The surrogates in Figure 4 indicate apparent correlative relationships with TOMS ozone, especially geopotential heights, zonal winds, and temperatures (including the vertical derivative of temperatures).

Figure 5 shows computed residuals involving five distinct models, beginning with a standard model (bold solid curve) that includes seasonality, linear trend, solar cycle, and the nonlagged EOF QBO winds. (The bold solid curve in Figure 5 is equivalent to the bold solid curve in Figure 1.) For each model, surrogates were deseasonalized and linearly detrended prior to regression.

The main result from Figure 5 is that all of the proxy cases clearly reduce residuals in zonal mean models. Reductions are generally moderate except in the SH middle and high latitudes involving MSU4 temperatures (long dashed curve). We note that there are many other dynamical surrogates of zonal mean total ozone not included in Figure 5. These other cases mirror the results of Figure 5 and were not shown.

5.2. Residuals: Zonally Asymmetric Models

In Figure 6 we again show RMS residuals, but now as a function of latitude and longitude for selected models using zonally asymmetric data. These models include optional ozone proxies ENSO(t), $\mathrm{P}_1(t)$, and $\mathrm{P}_2(t)$ (indicated at the top of each panel). In each case, before running trend model (1), $\mathrm{P}_1(t)$ and $\mathrm{P}_2(t)$ were deseasonalized and linearly detrended.

It was noted from Figure 3 that both vorticity and geopotential heights exhibit large total ozone correlation amplitudes at 200 hPa in midlatitudes year-round, and near 10 hPa in high latitudes (during winter-spring months). Hence, for either vorticity or geopotential heights, a logical choice would be to choose optional

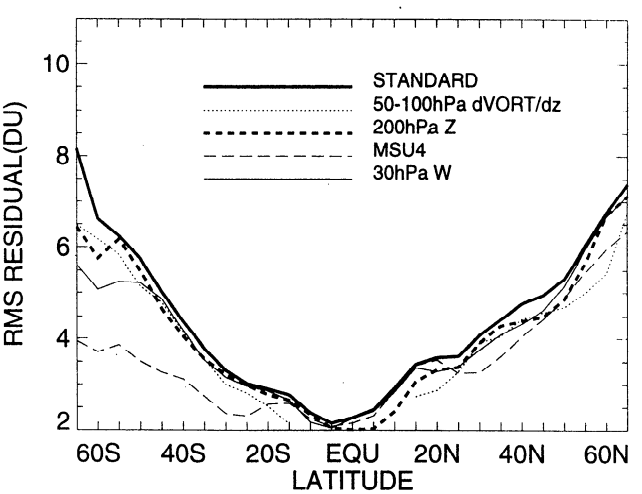

Figure 5. RMS residuals (in Dobson units) plotted as a function of latitude for several choices (indicated) of additional proxy $\mathrm{P}_1(t)$ in the zonal mean model used in Figure 1. Prior to regression, $\mathrm{P}_1(t)$ was deseasonalized and linearly detrended. The trend model used is $\Omega(t) = \alpha + \beta\, t + \gamma\ \mathrm{QBO}(t) + \delta\ \mathrm{solar}(t) + \zeta_1\ \mathrm{P}_1(t) + \mathrm{R}(t)$. (The bold solid curve is equivalent to the bold solid curve in Figure 1.)

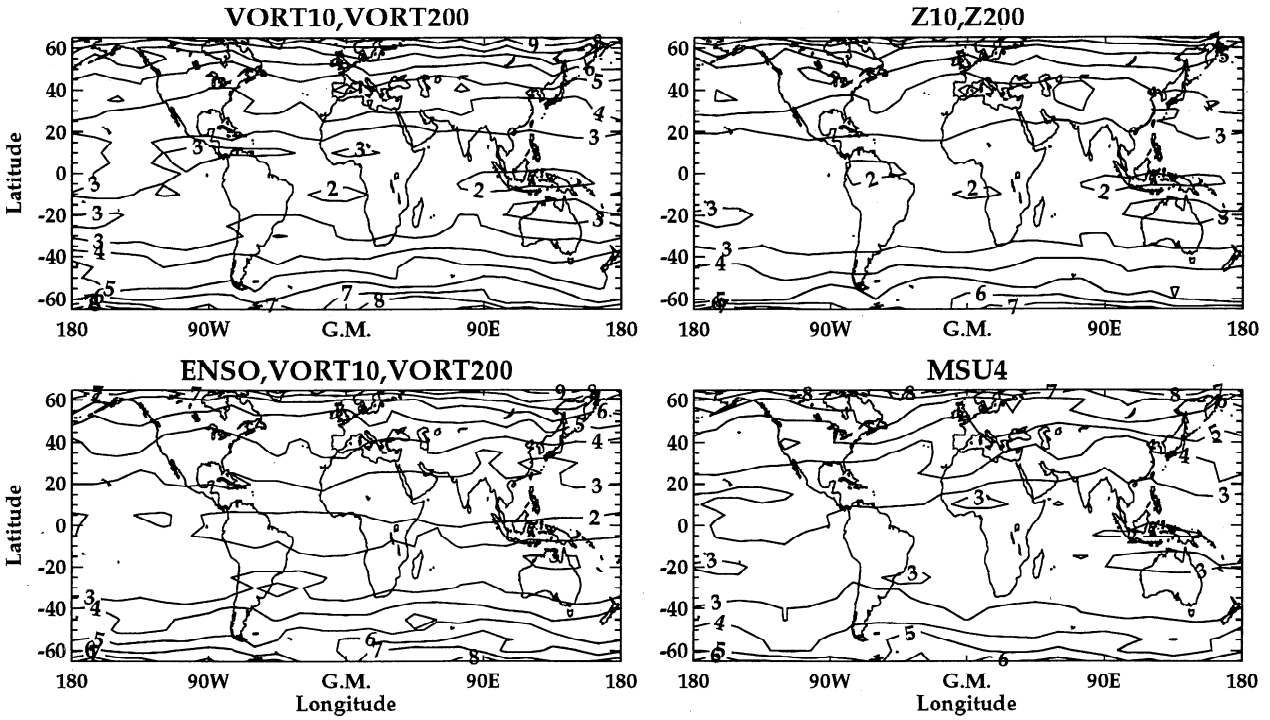

Figure 6. RMS residuals (in Dobson units) for a zonally asymmetric trend model with one, two, or three optional surrogates (indicated above each frame). The trend model used is $\Omega(t) = \alpha + \beta\, t + \gamma\ \mathrm{QBO}(t) + \delta\ \mathrm{solar}(t) + \epsilon\ \mathrm{ENSO}(t) + \zeta_1\ \mathrm{P}_1(t) + \zeta_2\ \mathrm{P}_2(t) + \mathrm{R}(t)$.

series at both 10 hPa ($\mathrm{P}_1(t)$) and 200 hPa ($\mathrm{P}_2(t)$) in (1).

Figure 6 indicates significant reductions in residuals by using relative vorticity at 10 and 200 hPa, either without ENSO (left column, top) or with ENSO (left column, bottom). (Compare these patterns with the larger residuals shown in Figure 2.) Inclusion of ENSO(t) again has only a small effect. Residuals using 10- and 200-hPa geopotential heights (right column, top) mask the basic results for vorticity. Using only MSU4 temperatures without ENSO (right column, bottom) does as well (perhaps slightly better) than the other three models.

All surrogate cases in Figure 6 clearly reduce residuals relative to a standard model (no optional surrogates), up to 50% in the SH. Surrogates also greatly smooth the zonal wave structures of residual fields. ENSO has little impact in doing either. In the next section we examine how surrogates affect zonal structures of ozone trends.

5.3. Impact of Surrogates on Ozone Zonal Trend Structures

Figure 7 shows annual mean (averaged over all 12 months) ozone trends and trend uncertainty fields involving four separate scenarios beginning with a standard zonally asymmetric model (top left) given by $\Omega(t) = \alpha + \beta\, t + \gamma\ \mathrm{QBO}(t) + \delta\ \mathrm{solar}(t) + \mathrm{R}(t)$. These selected cases were chosen in Figure 7 because they represent the general spread of model results using from zero to three (including ENSO) optional surrogates. Shading in Figure 7 indicates regions where the trend is not distinguishable from zero at the 5% significance level.

For the standard model, statistically significant negative trends are seen in the SH midlatitudes centered around 90°W and in the NH midlatitudes in three distinct (nonshaded) geographical regions. Largest ozone loss is in the SH high latitudes where maximum trend amplitudes are near 0°-30°W longitude with amplitudes ~10% decade^{-1}. Similar structures were shown for version 6 TOMS analyses by *Stolarski et al.* [1992].

The other three cases in Figure 7 incorporate additional (deseasonalized) surrogates in the standard trend model. The first case (upper right) includes both ENSO and nondetrended 500-hPa geopotential heights. As *Hood and Zaff* [1995] showed, NH climatological zonal wave structures in tropospheric (primarily 100 hPa) geopotential heights during January months indicated a likely stationary dynamical mechanism for producing the zonal wave structures observed in TOMS trends in winter. In Figure 7, relative to the standard model, 500-hPa heights show some zonal smoothing of TOMS zonal structures, but the effect is not large. In addition, there are small changes in ozone trend amplitudes of about +0.5 to +1% decade^{-1} in the NH middle and high latitudes.

In the study by *Chandra et al.* [1996], nondetrended MSU4 temperatures were used as an additional surrogate in a regression trend model for zonally asymmetric total ozone at 45°N under the hypothesis that decadal changes in MSU4 temperatures were in part dynamically induced. (There exists some proportion of radiative feedback effects of ozone on lower stratospheric temperatures.) Results indicated changes in TOMS ozone trends of +1 to +3% decade^{-1} after including

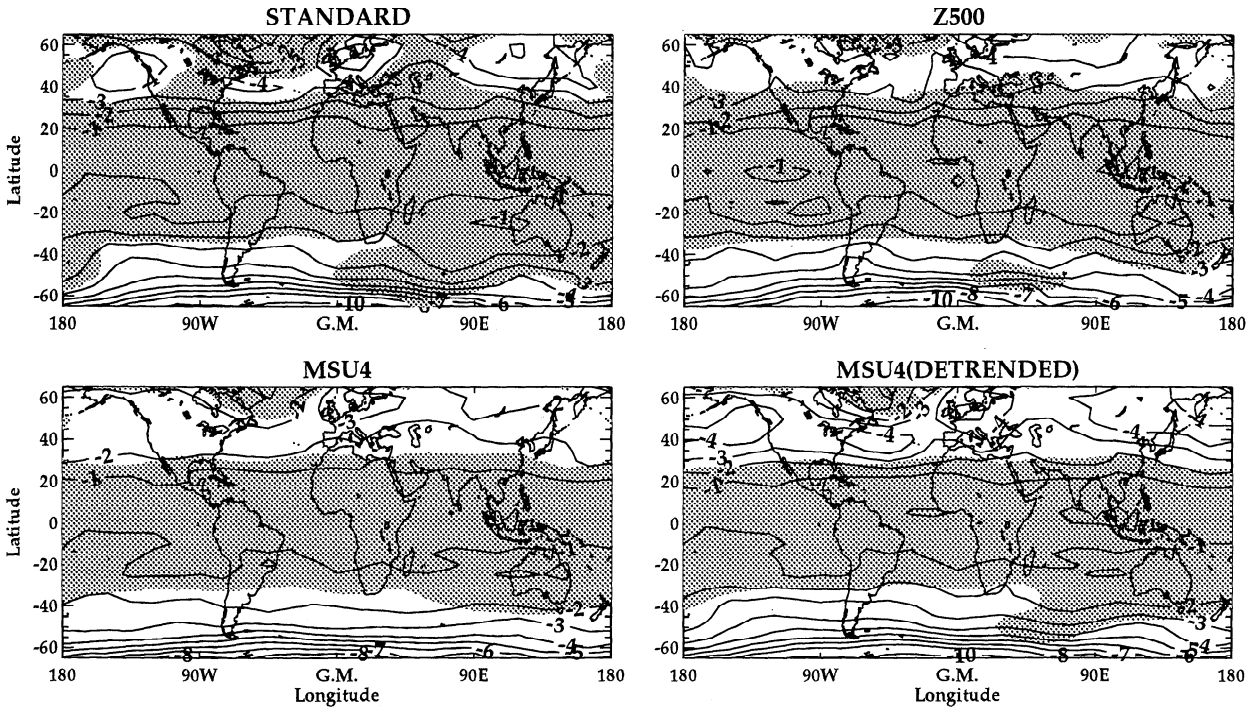

Figure 7. TOMS trends (in percent per decade) averaged over all 12 months for four model scenarios (see section 5.3). Shading indicates regions where trends are not different from zero at the 5% significance level.

MSU4 data. Our third global model in Figure 7 (lower left) similarly uses nondetrended MSU4 data. Aside from observable zonal smoothing in the NH, reductions in trends occur in the NH midlatitudes and SH high latitudes with changes of around +1 to +2% decade^{-1}. When MSU4 are detrended, ozone trends (lower right) show little change (at most, ~+1% decade^{-1}) from the standard model; however, using this extra proxy appreciably reduces residuals and the shaded uncertainty regions. Only nondetrended surrogates provide sizable changes in TOMS trends.

5.4. Implications for Chemical Transport Modeling of Ozone Trends

Figure 8 shows the same four 1979-1992 trend model analyses from Figure 7, but now zonally averaged and plotted for each month. We note that similar trend plots (not shown) generated by running all four models with zonal mean data have the same values (at most, ~0.5% decade^{-1} differences) as shown in Figure 8. For the standard model (upper left), large negative trends (around -14% decade^{-1}) associated with the Antarctic ozone hole are seen in the SH high latitudes poleward of 60°S around September-October. In the NH, largest trends are in midlatitudes during February, with values around -6% decade^{-1}. These trend results are nearly identical to version 7 TOMS trends shown by *McPeters et al.* [1996], despite their using 7-day zonal means and a longer 16-year data length (November 1978 through October 1994) that included Meteor 3 TOMS ozone after May 5, 1993. Partly because zonally asymmetric data were used in Figure 8, boundaries of the shaded uncertainty regions are slightly larger, ~0.5% decade^{-1} more negative than shaded regions for version 7 TOMS trends shown by *McPeters et al.* [1996].

An anomalous feature for both the standard and MSU4 cases is a SH low-latitude region of statistically significant negative trends of around -2% decade^{-1} from June through August. Examination of TOMS ozone indicates (figures not shown) that this trend anomaly is caused by a large drop in ozone centered in June 1992, coinciding exactly with the month of the primary eruption of Mount Pinatubo. However, a close examination shows that TOMS ozone is rapidly decreasing in April and May, which is around 2 months prior to the eruption. Hence the trend anomaly cannot be explained just from volcanic effects.

Of the three surrogate cases in Figure 8, largest reductions are for the nondetrended MSU4 proxy. Both nondetrended 500-hPa geopotential heights and MSU4 temperatures change NH midlatitude springtime trends by +1 to +2% decade^{-1}.

The important conclusions from Figure 8 are that (1) decadal variabilities in tropospheric and lower stratospheric dynamical quantities alter TOMS trends by at most 2-3% decade^{-1} anywhere for any month and (2) inclusion of optional surrogates reduces residuals and the size of the regions of uncertainty in ozone trends.

Figure 9 compares best estimated latitude versus month 1979-1992 total ozone trends from TOMS (top) with the Goddard 2-D heterogeneous chemistry and transport model (HCTM) [*Jackman et al.*, 1996]. The trends shown for TOMS are the same as in Figure 8 (bottom right) involving the deseasonalized detrended MSU4 temperature proxy. For the 2-D model, trends were computed from HCTM output data using regres-

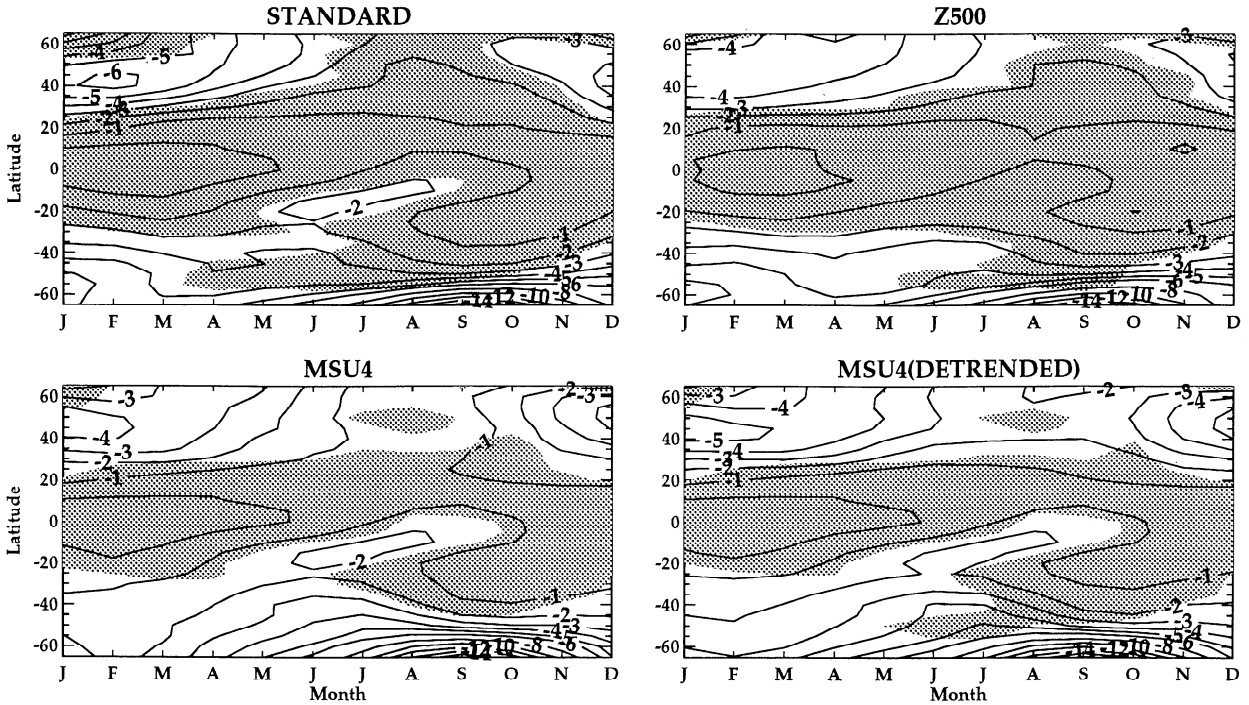

Figure 8. Same four trend model scenarios from Figure 7, but as latitude versus month with trends computed for each month and then zonally averaged (see section 5.3).

sion model (1) with seasonality, trend, and solar terms present. The Goddard model includes both solar cycle and volcanic aerosols (similar to *Solomon et al.* [1996]).

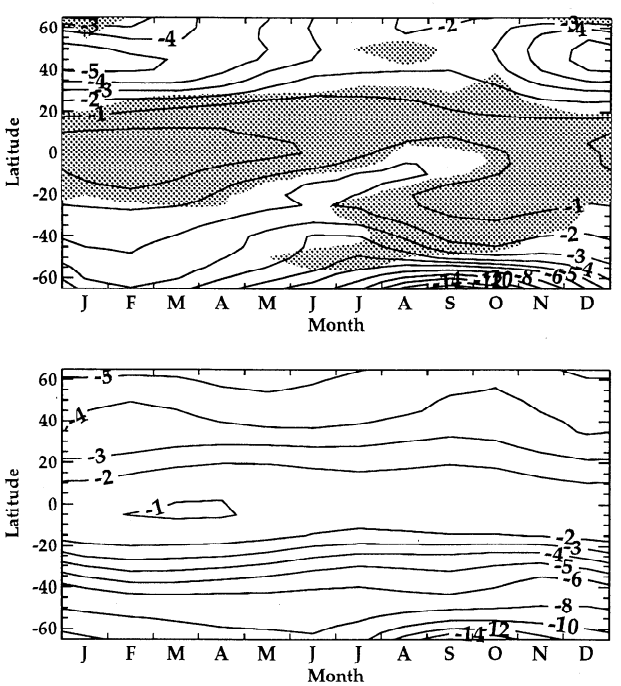

Figure 9. (top) Zonally averaged TOMS trends replotted from Figure 8, bottom right. (bottom) Goddard 2-D heterogeneous chemical transport model [*Jackman et al.*, 1996] total ozone trends (units in percent per decade) for 1979-1992 derived from (1) with seasonality, trend, and solar cycle terms present in the regression.

Aerosols and the solar cycle provide a source of interannual variability in the model.

HCTM trends in the SH high latitudes, similar to TOMS, show large seasonality, with maximum ozone loss in September-October. Seasonality in SH midlatitudes is weak, as is also generally true for TOMS trends. Seasonality in NH trends from the HCTM is again weak, yet despite the NH midlatitude maximum in spring from TOMS not being reproduced, trend amplitudes of TOMS and the model are nevertheless comparable. HCTM trends $\sim -3\%$ to -4% decade^{-1} in NH midlatitudes during spring are comparable to TOMS trends of around -3% to -5% decade^{-1}.

The important result from Figure 9 is that the HCTM trends agree favorably well in both hemispheres with TOMS, generally within 2-3% decade^{-1}. Inclusion of the possibility of decadal changes in dynamics (Figure 8) may yield yet smaller differences. We note that trend differences of 2-3% decade^{-1} are close to the critical trend uncertainties in TOMS (see shaded-region boundaries). In addition, such percentage changes may be caused just by unresolved interannual variabilities coupled with the data set length used.

6. Conclusions

This study has incorporated many combinations of dynamical surrogates of total ozone in both zonal mean and zonally asymmetric trend models. All models prescribed simple linear relationships between total ozone and surrogates, an assumption that is viable as a first approximation. Subtle nonlinear effects (beyond the scope of this study) were not considered.

The QBO proxy in trend models must be incorporated carefully. The EOF QBO winds (either lagged or not lagged) showed marked improvement from a standard model (model with only trend and solar cycle). Adding the EOF QBO winds to the standard model indicated long-term (14-year) RMS residual reductions of around 5 DU (~60-70% improvement) along the equator and between 2 and 3 DU in the midlatitudes of both hemispheres.

ENSO (Tahiti minus Darwin normalized sea level pressure time series) has little impact on long-term reduction of residuals. Inclusion of ENSO, either with or without other optional surrogates, has a comparatively small contributing reduction, ~1 DU or less in 14-year RMS values. This apparently stems from the episodic nature of ENSO.

Inclusion of additional ozone surrogates in the regressions considerably reduces residuals (up to 50% in the SH) from a basic model that included only trend, solar cycle, and EOF QBO. In zonal asymmetry models, optional surrogates also greatly reduce zonal asymmetries in residual fields. In all cases investigated, inclusion of surrogates reduces the size of uncertainty regions in trends. For zonal mean or zonally asymmetric trend models with one optional surrogate, a favorable choice is prefiltered (at least deseasonalized and detrended) lower stratospheric temperatures. Relative vorticity, potential vorticity, and geopotential heights all exhibit similar relationships with total ozone, with highest correlative behavior near 200 hPa (midlatitudes year-round) and 10 hPa (high latitudes in winter-spring months). For models incorporating these latter proxies, combined 10- and 200-hPa (or similar) pressure levels are effective in reducing global residuals.

HCTM ozone trends for all months in both hemispheres agree favorably well with TOMS trends, generally within 2-3% decade^{-1}. Inclusion of the possibility of decadal changes in dynamics may produce even smaller differences by changing TOMS trends by +1% to +2% decade^{-1}. Differences of 2% or 3% decade^{-1} are close to the critical trend uncertainties (boundaries of the shaded uncertainty regions) present in the TOMS trend analyses. In addition, such percentage changes may be caused just by interannual variabilities and length of data set. Omitting or adding just 1 year of data may produce similar percent differences in trends.

Appendix: Error Analysis

Errors in the coefficients $\alpha, \beta, \gamma, \delta, \epsilon, \zeta_1$, and ζ_2 in trend model (1) originate from all data input to the regression, that is, time series $\Omega(t)$ (which could also be geopotential heights, etc.), QBO(t), solar(t), ENSO(t), $P_1(t)$, and $P_2(t)$. Our method used for estimating errors in these coefficients was to first run the model once, generating the residual series R(t) at each grid point, and then run this same model N additional loops with random noise added to all of the original data fields. In our simulations we chose N=200. (When all 12 months are averaged together for regression coefficients, the effective number becomes 2400.) Random normally distributed (with mean zero) noise was added to add input data series. For total ozone (or geopotential heights, etc.) to which model (1) was applied, this noise was weighted by the latitudinally dependent seasonal climatology cycle. Noise in monthly mean total ozone and NCEP data was taken to be 2%. When MSU4 temperatures were included in (1) as a surrogate of ozone, a value of 1% in monthly averaged values was assumed.

In addition to these random errors, long-term uncertainties in calibration (for total ozone) and uncertainties associated with changes in assimilation methodology (for NCEP data) were also added to original series during each loop. These long-term trend uncertainties were taken to be uniformly distributed with parameter b, that is, with probability distribution $U(-b, b)$. For total ozone, b = 3% decade^{-1}, and for 500-hPa geopotential heights, b=10 m decade^{-1} was assumed. Normally distributed (with mean zero) noise during each loop was also arbitrarily added to QBO(t) (5%), solar(t) (3%), and ENSO(t) (5%).

Residual series R(t) was replaced during each loop with a series of random noise generated from the measured amplitude-random phase (MARP) approach of *Stanford and Ziemke* [1994], that is,

$$\mathrm{R}(t) = \sum_{\omega} A_m(\omega) \cos(\omega t - \phi), \qquad (A1)$$

where ω is angular frequency, $A_m(\omega)$ denotes measured frequency dependent amplitudes, and ϕ is a random uniformly distributed number from $-\pi$ to $+\pi$. During each loop, this form for R(t) was added to Ω as additional random noise.

Figure 10 shows one example of Monte Carlo generated trends in TOMS ozone at 150°E, 5°S, averaged

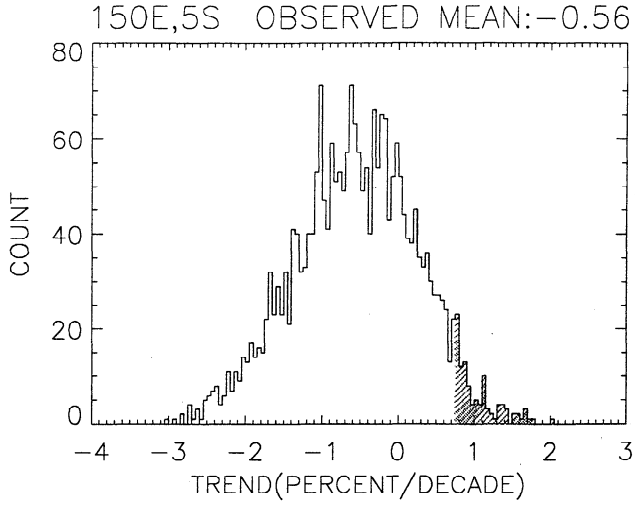

Figure 10. Histogram of Monte Carlo generated TOMS ozone trends at 150°E, 5°S. Units are percent per decade. This example corresponds to the shaded region in Figure 7, lower right. The trend model used is $\Omega(t) = \alpha + \beta\, t + \gamma$ QBO(t) $+ \delta$ solar(t) $+ \zeta_1$ MSU4(t) + R(t). The time series MSU4(t) were deseasonalized and linearly detrended prior to regression. The shaded region is the 5% critical region (see appendix).

over all 12 months, using deseasonalized and detrended MSU4 temperatures as an extra proxy. (This is the model used to generate the 5% significance level shaded regions shown in Figure 7 (lower right).) The null hypothesis used in our statistical tests for trends is that the true trend is zero. In an effort to show a trend different from zero, we must reject the null hypothesis. For testing at the 5% significance level we shade the 5% tail of the histogram where random trends are in a direction opposite in sign of the observed trend. Should the shaded tail region happen to include the value of zero trend, we reject the null hypothesis, thus concluding a trend different from zero at the 5% significance level. However, the example in Figure 10 is one that fails to reject the null hypothesis at the 5% significance level. That is, in order to reject the null hypothesis, the 5% shaded tail region must enclose zero along the horizontal axis, which it does not.

The Monte Carlo method used in this study to estimate errors in regression coefficients provides a highly powerful statistical simulation. Including the MARP technique to model residual series R(t) means that each randomly generated series will have a frequency spectrum identical to the original measured series, thus providing a physical constraint that multivariate approaches cannot replicate.

Acknowledgments. We wish to thank the members of the NASA TOMS Nimbus Experiment and Information Processing Teams for providing the version 7 TOMS data. We greatly acknowledge C. Jackman and D. Considine for helpful discussions and for providing data from the Goddard 2-D heterogeneous chemistry and transport model. A portion of this work was performed while J. Ziemke held a National Research Council–Goddard Space Flight Center Research Associateship.

References

Andrews, D. G., J. R. Holton, and C. B. Leovy, *Middle Atmosphere Dynamics*, 489 pp., Academic, San Diego, Calif., 1987.

Bowman, K. P., Global patterns of the quasi-biennial oscillation in total ozone, *J. Atmos. Sci., 46*, 3328–3343, 1989.

Chandra, S., and R. S. Stolarski, Recent trends in stratospheric total ozone: Implications of dynamical and El Chichon perturbations, *Geophys. Res. Lett., 18*, 2277–2281, 1991.

Chandra, S., C. Varotsos, and L. E. Flynn, The midlatitude total ozone trends in the northern hemisphere, *Geophys. Res. Lett., 23*, 555-558, 1996.

Dobson, G. M. B., and D. N. Harrison, Measurements of the amount of O_3 in the earth's atmosphere and its relation to other geophysical conditions, I, *Proc. R. Soc. London A, 110*, 660–693, 1926.

Dobson, G. M. B., A. W. Brewer, and B. M. Cwilong, Meteorology of the lower stratosphere, *Proc. R. Soc. London A, 185*, 144–175, 1946.

Farman, J. C., B. G. Gardiner, and J. D. Shanklin, Large losses of total ozone in Antarctica reveal seasonal ClO_x / NO_x interaction, *Nature, 35*, 207–210, 1985.

Garcia, R. R., and M. L. Salby, Transient response to localized episodic heating in the tropics, II, Far-field behavior, *J. Atmos Sci., 44*, 499–530, 1987.

Hamilton, K., Interhemispheric asymmetry and annual synchronization of the ozone quasi-biennial oscillation, *J. Atmos. Sci., 46*, 1019–1025, 1989.

Hasebe, F., A global analysis of the fluctuations in total ozone, II, Non-stationary annual oscillation, quasi-biennial oscillation, and long-term variations in total ozone, *J. Meteorol. Soc. Jpn., 58*, 104–117, 1980.

Hasebe, F., Quasi-biennial oscillations of ozone and diabatic circulation in the equatorial stratosphere, *J. Atmos. Sci., 51*, 729–745, 1994.

Hood, L. L., and D. A. Zaff, Lower stratospheric stationary waves and the longitude dependence of ozone trends in winter, *J. Geophys. Res., 100*, 25,791–25,800, 1995.

Jackman, C. H., E. L. Fleming, S. Chandra, D. B. Considine, and J. E. Rosenfield, Past, present, and future modeled ozone trends with comparisons to observed trends, *J. Geophys. Res., 101*, 28,753–28,767, 1996.

Kiehl, J. T., B. A. Boville, and B. P. Briegleb, Response of a general circulation model to a prescribed Antarctic ozone hole, *Nature, 332*, 501–504, 1988.

Kutzbach, J. E., Empirical eigenvectors of sea-level pressure, surface temperature and precipitation complexes over North America, *J. Appl. Meteorol., 6*, 791–802, 1967.

Lait, L. R., M. R. Schoeberl, and P. A. Newman, Quasi-biennial modulation of the Antarctic ozone depletion, *J. Geophys. Res., 94*, 11,559–11,571, 1989.

McPeters, R. D., S. M. Hollandsworth, L. E. Flynn, and J. R. Herman, Long-term ozone trends derived from the 16-year combined Nimbus 7/Meteor 3 TOMS version 7 record, *Geophys. Res. Lett., 23*, 3699–3702, 1996.

Miller, A. J., R. M. Nagatani, G. C. Tiao, X. F. Niu, G. C. Reinsel, D. Wuebbles, and K. Grant, Comparisons of observed ozone and temperature trends in the lower stratosphere, *Geophys. Res. Lett., 19*, 929–932, 1992.

Murgatroyd, R. J., and F. Singleton, Possible meridional circulations in the stratosphere and mesosphere. *Q. J. R. Meteorol. Soc., 87*, 125–135, 1961.

Newman, P. A., and W. J. Randel, Coherent ozone-dynamical changes during the southern hemisphere spring, 1979-1986, *J. Geophys. Res., 93*, 12,585–12,606, 1988.

Niu, X., J. E. Frederick, M. L. Stein, and G. C. Tiao, Trends in column ozone based on TOMS data: Dependence on month latitude and longitude, *J. Geophys. Res., 97*, 14,661–14,669, 1992.

Randel, W. J., and J. B. Cobb, Coherent variations of monthly mean total ozone and lower stratospheric temperature, *J. Geophys. Res., 99*, 5433–5447, 1994.

Randel, W. J., F. Wu, J. M. Russell III, J. W. Waters, and L. Froidevaux, Ozone and temperature changes in the stratosphere following the eruption of Mount Pinatubo, *J. Geophys. Res., 100*, 16,753–16,764, 1995.

Reed, R. J., The role of vertical motions in ozone-weather relationships, *J. Meteorol., 7*, 263–267, 1950.

Reinsel, G. C., G. C. Tiao, D. J. Wuebbles, J. B. Kerr, A. J. Miller, R. M. Nagatani, L. Bishop, and L. H. Ying, Seasonal trend analysis of published ground-based and TOMS total ozone data through 1991, *J. Geophys. Res., 99*, 5449–5464, 1994.

Shine, K. P., On the modeled thermal response of the Antarctic stratosphere to a depletion of ozone, *Geophys. Res. Lett., 13*, 1331–1334, 1986.

Solomon, S., R. W. Portmann, R. R. Garcia, L. W. Thomason, L. R. Poole, and M. P. McCormick, The role of aerosol variations in anthropogenic ozone depletion at northern midlatitudes, *J. Geophys. Res., 101*, 6713–6727, 1996.

Stanford, J. L., and J. R. Ziemke, Field (map) statistics, in *Statistical Methods for Physical Science*, edited by J. L. Stanford and S. B. Vardeman, pp. 457–479, Academic, San Diego, Calif., 1994.

Stolarski, R. S., P. Bloomfield, R. D. McPeters, and J. R. Herman, Total ozone trends deduced from Nimbus 7 TOMS data, *Geophys. Res. Lett., 18*, 1015–1018, 1991.

Stolarski, R., R. Bojkov, L. Bishop, C. Zerefos, J. Staehelin, and J. Zawodny, Measured trends in stratospheric ozone, *Science, 256*, 342–349, 1992.

Stone, E. M., J. L. Stanford, J. R. Ziemke, D. R. Allen, F. W. Taylor, C. D. Rodgers, B. N. Lawrence, E. F. Fishbein, L. S. Elson, and J. W. Waters, Space-time integrity of improved stratospheric and mesospheric sounder and microwave limb sounder temperature fields at Kelvin wave scales, *J. Geophys. Res., 100*, 14,089–14,096, 1995.

Wallace, J. M., R. L. Panetta, and J. Estberg, Representation of the equatorial stratospheric quasi-biennial oscillation in EOF phase space, *J. Atmos. Sci., 50*, 1751–1762, 1993.

Wirth, V., Quasi-stationary planetary waves in total ozone and their correlation with lower stratospheric temperature, *J. Geophys. Res., 98*, 8873–8882, 1993.

World Meteorological Organization/UNEP, Scientific assessment of ozone depletion: 1994, WMO Global Ozone Research and Monitoring Project, *Rep. 37*, Geneva, Switzerland, 1995.

S. Chandra, R. D. McPeters, and P. A. Newman, NASA Goddard Space Flight Center, Code 916, Greenbelt, MD 20771. (e-mail: chandra@chapman.gsfc.nasa.gov, mcpeters@wrabbit.gsfc.nasa.gov, newman@notus.gsfc.nasa.gov)

J. R. Ziemke, National Research Council, NASA Goddard Space Flight Center, Code 916, Greenbelt, MD 20771. (e-mail: ziemke@jwocky.gsfc.nasa.gov)

(Received September 20, 1996; revised December 3, 1996; accepted December 3, 1996.)